

Sound-mediated dynamic correlations between colloidal particles in a quasi-one-dimensional channel

D Frydel and H Diamant

Raymond and Beverly Sackler School of Chemistry, Tel Aviv University, Tel Aviv 69978, Israel

E-mail: hdiamant@tau.ac.il

Abstract. We study the hydrodynamic interactions between colloids suspended in a compressible fluid inside a rigid channel. Using lattice-Boltzmann simulations and a simplified hydrodynamic theory, we find that the diffusive dynamics of density perturbations (sound) in the confined fluid give rise to particle correlations of exceptionally long spatial range and algebraic temporal decay. We examine the effect of these sound-mediated correlations on two-particle dynamics and on the collective dynamics of a quasi-one-dimensional suspension.

1. Introduction

Particles embedded in an unbounded fluid are dynamically correlated by hydrodynamic interactions that decay like $1/r$ (where r denotes the separation between particles) [1]. This result is understood in terms of the fundamental solution to the steady-state Stokes equation, $\eta \nabla^2 \mathbf{u} = \nabla p - \mathbf{b} \delta(\mathbf{r})$, supplemented by the fluid-incompressibility condition $\nabla \cdot \mathbf{u} = 0$. Here \mathbf{u} is the flow velocity field, p the pressure field, \mathbf{b} a point force, and η the shear viscosity. It follows from the first equation that the vorticity, $\nabla \times \mathbf{u}$, satisfies the Laplace equation, leading in the case of an unbounded fluid to the $1/r$ slow decay of the velocity field. When particles are confined to a quasi-one-dimensional (q1D) channel, however, these long-range dynamic correlations are cut off [2], the screening being attributed to dissipation at the fluid-solid interface, i.e., to the loss of fluid momentum at the channel boundaries. The resulting screening length is comparable to the channel width.

The dissipative effect of the boundaries can be incorporated through an additional friction term in an “effective fluid” model [3, 4], $\eta \nabla^2 \mathbf{u} = \rho_0 \xi \mathbf{u} + \nabla p - \mathbf{b} \delta(\mathbf{r})$. In the extra term ρ_0 is the fluid mass density and ξ an effective friction coefficient. The parameter ξ has units of inverse time and characterizes the rate of momentum loss to the boundaries. It can be estimated, therefore, as the inverse of the time it takes fluid momentum to diffuse to the channel boundary, $\xi \sim \nu/h^2$, $\nu = \eta/\rho_0$ being the kinematic shear viscosity and h the channel width. This simplified, phenomenological approach has been shown by simulations [5, 6, 7, 8] and analytical calculations [9] to correctly reproduce the qualitative behavior of confined fluids. The modified Stokes equation leads to a Helmholtz equation for the vorticity, whose regular solutions are exponentially screened functions. Yet, the friction that suppresses the vorticity (transverse fluid stress) does not similarly suppress the pressure field (longitudinal fluid stress) emanating from a locally applied force. Consequently, the application of a localized force generates a long-range pressure distribution, which may give rise to long-range flows and forces on embedded particles. For example, in a q2D suspension confined between two plates, the pressure distribution creates

hydrodynamic interactions that decay like $1/r^2$, while the $1/r$ correlations due to transverse momentum transfer are cut off [10]. Thus, although the hydrodynamic interactions in the q2D system remain long-ranged, the very mechanism for correlations changes [11]. In the case of a q1D channel, the pressure generated by a localized force far along the channel is constant and, therefore, does not produce long-range forces. Thus, within the Stokes description of a steady incompressible flow, in a q1D rigid channel long-range hydrodynamic interactions arise neither from transverse stresses nor from longitudinal ones, and the correlation between particles is screened, the screening length being proportional to the channel width [2].

The omission of compressibility, and with it of compression (longitudinal sound) modes, is usually justified for unbounded fluids, where the effects of sound are short-lived. The short propagation time to any reasonable distance r , $\tau_s \sim r/c_s$, is a result of the large speed of sound, $c_s \sim 10^3$ m/s for ordinary liquids such as water. The effect of sound on the short-time hydrodynamic interactions in unconfined suspensions was addressed in earlier works [12, 13, 14]. The corresponding effects are subtle and short-lived, quickly taken over by the fully established hydrodynamic interaction due to transverse flow.

In confined geometries, however, the behavior of sound modes qualitatively changes. Inclusion of fluid compressibility has been found to lead to a velocity autocorrelation function of a confined particle, which decays with time only algebraically, with a negative long-time tail [5, 6, 7, 15]. [In the case of a q1D channel the decay is $\sim (-t^{-3/2})$.] Thus, under confinement, sound acquires long-time memory without a well-defined relaxation time, and the incompressibility assumption loses, at least in principle, its justification. Informed by this result, one suspects that the long memory of sound modes may play a role in the dynamic correlations between different particles in a channel: since sound may propagate to long distances, the resulting correlations will be long-ranged, and the algebraic temporal decay will endow these interactions with a long-time memory. This novel mechanism for correlations challenges the conventional wisdom described above, according to which fluid-mediated correlations in a rigid channel are exponentially screened. The question that comes to mind is whether the long-time memory of sound is sufficiently significant to be observed experimentally and to undermine predictions of the theories based on the assumption of incompressibility. We remind that the algebraic temporal decay of sound modes in a channel does not imply that sound is capable of causing steady rearrangement of the fluid. The integrated effect of the $t^{-3/2}$ tail decays as $t^{-1/2}$, which is very slow, but still implies that at infinite time (the steady-state limit) all perturbations due to sound eventually vanish.

In a recent Letter [16] we have demonstrated that the heuristic arguments given above are correct — namely, the diffusive, slowed-down sound modes of a fluid confined in a rigid channel mediate long-range and long-time velocity correlations between suspended particles. In the present publication we report detailed findings concerning the compressive response of the fluid and its effect on particles, which were not included in that brief publication. Two tools are employed and compared: simplified analytical calculations and lattice-Boltzmann simulations. We assume no-slip boundary conditions at the fluid-particle interface and consider either slip or no-slip boundary conditions at the channel boundaries. Fluid dynamics in a q1D channel strongly depends on the boundary conditions imposed at the edges of the channel [17]. In the calculations we assume an infinitely long channel with a vanishing flow velocity at the edges. In the simulation we take a sufficiently long channel, such that all the temporal results presented below are insensitive to the system size. Further details of the simulations can be found in Ref. [16].

2. Dynamics of fluid density perturbations

2.1. Unbounded fluid

We begin by revisiting the compressive response of an unbounded Newtonian fluid to an impulsive force [18], to which we will later compare the case of a fluid confined in a channel [15, 19].

Isothermal fluid dynamics [20] is governed by the momentum-conservation Navier–Stokes equation,

$$\rho \left[\partial_t \mathbf{u} + (\mathbf{u} \cdot \nabla) \mathbf{u} \right] = -\nabla p + \eta \nabla^2 \mathbf{u} + (\eta_v + \eta/3) \nabla (\nabla \cdot \mathbf{u}) + \mathbf{f}, \quad (1)$$

and the mass-conservation equation,

$$\partial_t \rho + \nabla \cdot (\rho \mathbf{u}) = g. \quad (2)$$

In these equations ρ is the fluid density field, \mathbf{f} an external force density, and η and η_v are the shear and volume viscosities, respectively. The function g could represent, for example, a mass monopole, $m\delta(\mathbf{r} - \mathbf{r}_0)$, where at the point \mathbf{r}_0 fluid is generated or lost, or a mass dipole, $-\mathbf{d} \cdot \nabla \delta(\mathbf{r} - \mathbf{r}_0)$, where fluid is at the same time created and lost, thus globally conserving mass but generating a flow.

The hydrodynamic equations are linearized by neglecting the convective term, $(\mathbf{u} \cdot \nabla) \mathbf{u}$, and separating the thermodynamic variables into equilibrium and small perturbation parts, $\rho(\mathbf{r}, t) = \rho_0 + \delta\rho(\mathbf{r}, t)$ and $p(\mathbf{r}, t) \simeq p_0 + (\partial p / \partial \rho) \delta\rho = p_0 + c_s^2 \delta\rho(\mathbf{r}, t)$. The resulting linearized equations read

$$\rho_0 \partial_t \mathbf{u} = -c_s^2 \nabla \delta\rho + \eta \nabla^2 \mathbf{u} + (\eta_v + \eta/3) \nabla (\nabla \cdot \mathbf{u}) + \mathbf{f}, \quad (3)$$

$$\partial_t \delta\rho + \rho_0 \nabla \cdot \mathbf{u} = g. \quad (4)$$

When dealing with sound, it is convenient to decompose the linearized equations into transverse and longitudinal components (the so called Helmholtz decomposition), $\mathbf{u} = \mathbf{u}^T + \mathbf{u}^L$, which satisfy $\nabla \cdot \mathbf{u}^T = 0$ and $\nabla \times \mathbf{u}^L = 0$. The decomposition yields

$$\rho_0 \partial_t \mathbf{u}^T = \eta \nabla^2 \mathbf{u}^T + \mathbf{f}^T, \quad (5)$$

and

$$\rho_0 \partial_t \mathbf{u}^L = -c_s^2 \nabla \delta\rho + (\eta_v + 4\eta/3) \nabla^2 \mathbf{u}^L + \mathbf{f}^L, \quad (6a)$$

$$\partial_t \delta\rho + \rho_0 \nabla \cdot \mathbf{u}^L = g, \quad (6b)$$

where we have used the identity $\nabla (\nabla \cdot \mathbf{u}) = \nabla^2 \mathbf{u}^L$. After separating the force-density field into transverse and longitudinal components, $\mathbf{f} = \mathbf{f}^T + \mathbf{f}^L$, the two flows become independent. The sound is associated with the longitudinal flow, which is coupled dynamically to the density — i.e., the sound modes characterize the propagation and relaxation of a density perturbation.

The time evolution of a density perturbation is obtained by taking the divergence of Eq. (6a) and then transforming it using the mass-conservation equation, Eq. (6b),

$$\partial_t^2 \delta\rho = c_s^2 \nabla^2 \delta\rho + 2\Gamma \nabla^2 \partial_t \delta\rho - \mathbf{b} \cdot \nabla \delta(\mathbf{r}) \delta(t). \quad (7)$$

In Eq. (7) $\Gamma = \frac{1}{2} \frac{\eta_v + 4/3\eta}{\rho_0}$, and we have set $g = 0$ and the force density to an impulsive point force, $\mathbf{f} = \mathbf{b} \delta(\mathbf{r}) \delta(t)$. Note that the application of the impulsive point force generates a momentary mass dipole in the equation for the density, $-(\mathbf{b} \delta(t)) \cdot \nabla \delta(\mathbf{r})$. Equation (7) represents a damped wave equation with a damping parameter Γ . If $\Gamma = 0$, we retrieve a wave equation for $\delta\rho$,

and if $c_s = 0$, we obtain a diffusion equation for $\partial_t \delta \rho$. Upon Fourier-transforming the spatial coordinates, Eq. (7) becomes

$$\partial_t^2 \delta \rho_k + (2\Gamma k^2) \partial_t \delta \rho_k + (c_s^2 k^2) \delta \rho_k = -i\mathbf{k} \cdot \mathbf{b} \delta(t),$$

whose solution reads

$$\delta \rho_k(t) = \frac{-i\mathbf{k} \cdot \mathbf{b} e^{-\Gamma k^2 t}}{\sqrt{c_s^2 k^2 - \Gamma^2 k^4}} \sin\left(t \sqrt{c_s^2 k^2 - \Gamma^2 k^4}\right). \quad (8)$$

If $c_s^2 - \Gamma^2 k^2 > 0$, the density perturbation propagates as a decaying wave. If, on the other hand, $c_s^2 - \Gamma^2 k^2 < 0$, the sine becomes a hyperbolic sine, and the density perturbation propagates diffusively. The crossover between these two behaviors occurs above a wavelength $\sim \Gamma/c_s$. For water $\Gamma/c_s \approx 1$ nm, while a typical colloid diameter is $\sigma \approx 10^3$ nm. Therefore, particle correlations arising from sound are mediated by essentially underdamped wave-like modes. In this large-wavelength limit, $k^{-1} \gg \Gamma/c_s$, Eq. (8) further simplifies to

$$\delta \rho_k(t) \approx \frac{-i\mathbf{k} \cdot \mathbf{b} e^{-\Gamma k^2 t}}{c_s k} \sin(c_s k t). \quad (9)$$

Figure 1 shows a snapshot of the density perturbation, generated a certain given time after the application of an impulsive force inside an unbounded fluid. We compare the result of a lattice-Boltzmann simulation, where the force is applied to a rigid spherical particle, with Eq. (8) for a point force. The analytical calculation reproduces all the features of the simulation, with a quantitative discrepancy that can be ascribed to the finite particle size in the simulation.

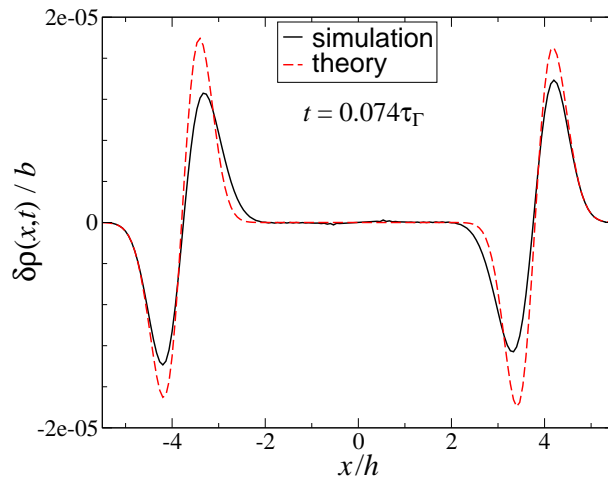


Figure 1. Snapshot of the density perturbation generated by an impulsive force in an unbounded fluid. The force is applied at the origin in the positive x direction. Lattice-Boltzmann simulation result (where the force is applied to a rigid sphere of diameter σ) is compared with the analytical one for a point force [Fourier-inverted Eq. (8)]. The snapshot is taken $0.074\tau_\Gamma$ after the impulse, where $\tau_\Gamma = h^2/\Gamma$ and $h = 1.5\sigma$.

2.2. Channel with slip boundary conditions

For a fluid confined in a channel with slip boundary conditions, we neglect variations of the density over the channel cross-section and consider only the direction along the channel, x .

Equation (7) is then rewritten as

$$\partial_t^2 \delta \rho = c_s^2 \delta \rho'' + 2\Gamma \delta \partial_t \rho'' - \frac{b}{h^2} \delta'(x) \delta(t),$$

where a prime indicates differentiation with respect to x , and an impulse is evenly distributed over the cross-sectional area of a square channel of side h . In the long wavelength limit the solution takes the form,

$$\delta \rho \approx \frac{b}{2c_s h^2} \left(\frac{e^{-(x-c_s t)^2/(4\Gamma t)}}{\sqrt{4\pi\Gamma t}} - \frac{e^{-(x+c_s t)^2/(4\Gamma t)}}{\sqrt{4\pi\Gamma t}} \right). \quad (10)$$

There are two signals propagating with the speed of sound in opposite directions. In addition, each signal spreads out diffusively with diffusion coefficient Γ . Figure 2 shows density perturbation snapshots generated by an impulse applied at the center and along a square channel with slip boundary conditions. Lattice-Boltzmann simulation results, where the impulse is applied to a spherical particle, agree well with Eq. (10).

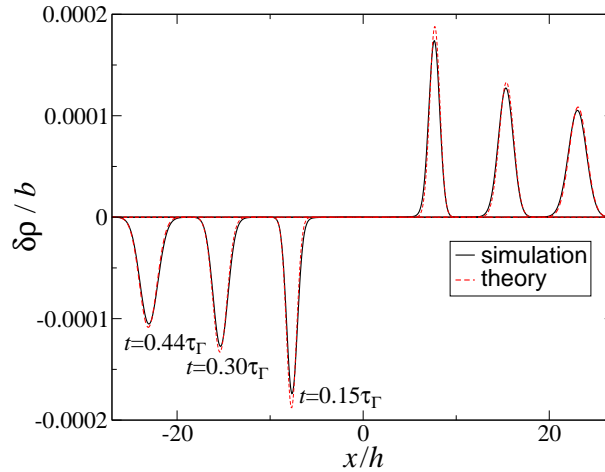


Figure 2. Three snapshots of a density perturbation for a fluid in a square channel with slip boundary conditions. An impulsive force is applied along the channel axis in the positive x direction. Lattice-Boltzmann simulation results (where the force is applied to a rigid sphere of diameter σ) are compared with the analytical ones for a force distributed uniformly over the square cross-section of side $h = 1.5\sigma$ [Eq. (10)]. The time unit is $\tau_\Gamma = h^2/\Gamma$.

2.3. Channel with no-slip boundary conditions

To account for no-slip boundary conditions at the channel walls, we introduce an effective friction term, $(-\rho_0 \xi \mathbf{u}^L)$, to the right-hand side of Eq. (6a). This leads to an extra term, $(-\xi \partial_t \delta \rho)$, in Eq. (7). Thus, neglecting again density variations transverse to the channel axis, we have the effective 1D equation,

$$\partial_t^2 \delta \rho = c_s^2 \delta \rho'' + 2\Gamma \partial_t \delta \rho'' - \xi \partial_t \delta \rho - \frac{b}{h^2} \delta'(x) \delta(t).$$

For the friction coefficient (rate of momentum loss to the walls) we take $\xi = \alpha \nu / h^2$, where $\nu = \eta / \rho_0$ is the kinematic shear viscosity, and α a geometrical prefactor, dependent on the

shape of the channel cross-section. (The value of α can be determined from the resistance of the channel to a steady pressure-driven flow, e.g., $\alpha \simeq 28.454$ for a square cross-section and $\alpha = 36$ for a circular one [1, 9].)

In Fourier space the solution reads

$$\delta\rho_k(t) = \frac{b}{h^2} \frac{(-ik)e^{-(\Gamma k^2 + \alpha\nu/2h^2)t}}{\sqrt{c_s^2 k^2 - (\Gamma k^2 + \alpha\nu/2h^2)^2}} \sin\left(t\sqrt{c_s^2 k^2 - (\Gamma k^2 + \alpha\nu/2h^2)^2}\right). \quad (11)$$

The corresponding signal propagates with underdamped oscillations only for a narrow range of small wavelengths, satisfying

$$\frac{c_s}{2\Gamma} \left(1 - \sqrt{1 - \frac{2\Gamma}{D_s}}\right) < k < \frac{c_s}{2\Gamma} \left(1 + \sqrt{1 - \frac{2\Gamma}{D_s}}\right), \quad (12)$$

where $D_s = c_s^2 h^2 / (\alpha\nu)$ is the sound diffusion coefficient. Hence, the friction at the walls transforms the large-scale dynamics from oscillating to diffusive. In the large-wavelength limit Eq. (11) reduces to

$$\delta\rho_k(t) \approx \left(\frac{b}{\alpha\nu}\right) (-ik) e^{-D_s k^2 t}, \quad (13)$$

which in real space reads,

$$\delta\rho \approx \frac{b}{\alpha\nu} \frac{2}{\sqrt{\pi}} \frac{x e^{-x^2/4D_s t}}{(4D_s t)^{3/2}}. \quad (14)$$

Thus, at large distances the density perturbation evolves as a diffusive dipolar signal.

Figure 3 shows snapshots of the density perturbation propagating in a square channel with no-slip boundary conditions. The wave-like propagation quickly disappears and the perturbation continues to evolve diffusively. Once again, the simplified 1D theory is found to qualitatively reproduce all the features seen in the lattice-Boltzmann simulation [21].

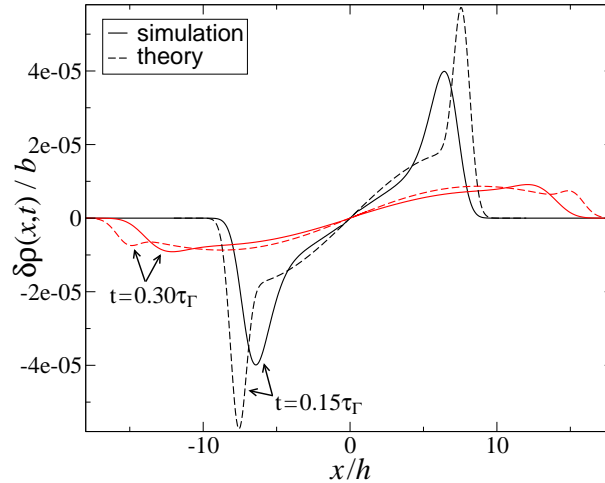


Figure 3. Two snapshots of a density perturbation for a fluid in a square channel with no-slip boundary conditions. An impulsive force is applied along the channel axis in the positive x direction. Lattice-Boltzmann simulation results (where the force is applied to a rigid sphere of diameter σ) are compared with the analytical ones for a force distributed uniformly over the square cross-section of side $h = 1.5\sigma$ (Fourier-inverted Eq. (11), multiplied by a factor of 2 [21]). The time unit is $\tau_\Gamma = h^2/\Gamma$.

3. Velocity cross-correlation function

Section 2 has been concerned with the dynamics of density perturbations in a viscous fluid. We now proceed to examine the effect of this dynamic response on particles suspended in the fluid.

Hydrodynamics represents the fluid as a continuous medium. Its discrete structure is revealed when a large particle immersed in the fluid undergoes Brownian motion due to large number of collisions with the much smaller fluid particles. Fluid particles impart momentum to the large particle, and the particle, in its turn, returns momentum to the fluid by setting off large-scale fluid flows. These flows lead to fluid-mediated correlations between the large particles. The flows can be decomposed, according to Eqs. (5) and (6), into transverse and longitudinal components. The present work is concerned with correlations caused by density perturbations, and so we focus on the role of longitudinal flows. As noted in Sec. 1, transverse flows in a rigid channel are screened at distances larger than the channel width and do not contribute to long-range correlations.

To visualize these flow-mediated correlations, we show in Fig. 4 velocity cross-correlation functions between two isolated particles, as obtained from lattice-Boltzmann simulations for three different systems: an unbounded fluid, a fluid in a square channel with slip boundary conditions, and a fluid in a square channel with no-slip boundary conditions. The cross-correlation function,

$$C(t, d) = \left\langle V_1(0)V_2(t) \right\rangle_d,$$

measures ensemble-averaged correlations between the velocities of two particles, V_1 and V_2 , separated by a distance d . In all three cases we take the two velocities to be oriented along the line that connects the centers of the two particles. To avoid the time-consuming fluctuating simulations and averaging procedure, we employ instead a deterministic measurement of $C(t, d)$ based on the linear response of the two-particle system. The equivalence of the two measurements is guaranteed by the fluctuation-dissipation theorem [22]. The procedure goes as follows. For $t < 0$ both particles are at rest, $V_1(t) = V_2(t) = 0$. At $t = 0$ we apply an instantaneous force to particle 1 by assigning it a finite initial velocity, $V_1(t = 0) = V_0$. As time evolves, $V_2(t)$ responds to the perturbation set off by particle 1. The velocity cross-correlation function is then obtained as

$$\frac{C(t, d)}{k_B T} = \frac{1}{M} \frac{V_2(t)}{V_1(0)},$$

where M is the particle mass and $k_B T$ the thermal energy.

In Fig. 4 we see that in all three systems there is a finite incipient time required for the signal to reach particle 2. This time is roughly d/c_s . The leading signal in the channels is larger than that in the unbounded fluid, because the perturbation is guided along the channel rather than spreading in 3D. At larger inter-particle distances, however, that signal is suppressed in the case of a rigid channel with no-slip boundary conditions because of the diffusive nature of sound. (See Fig. 5.)

The correlations at long times are very different for the three systems. In the unbounded case the correlation is governed by a positive algebraic tail, $\sim t^{-3/2}$. This is a manifestation of the well known long-time tails arising from the 3D diffusion of vorticity (monopolar transverse flow) [22]. In the rigid (no-slip) channel correlations due to transverse flows are screened, and the long-time correlation is governed by a negative algebraic tail, $\sim (-t^{-3/2})$. This is a result of the 1D diffusion of sound (dipolar longitudinal flow) presented in Sec. 2. By contrast, in the case of a channel with slip boundary conditions, the longitudinal signal propagates acoustically, making the correlation vanish exponentially fast once the signal has passed particle 2.

We next focus on the sound-mediated correlations in a rigid channel with no-slip boundary conditions. Figure 5 shows $C(t, d)$ for different separations d . The structure is similar for the different separations. There is the incipient time required for the leading signal to reach the other

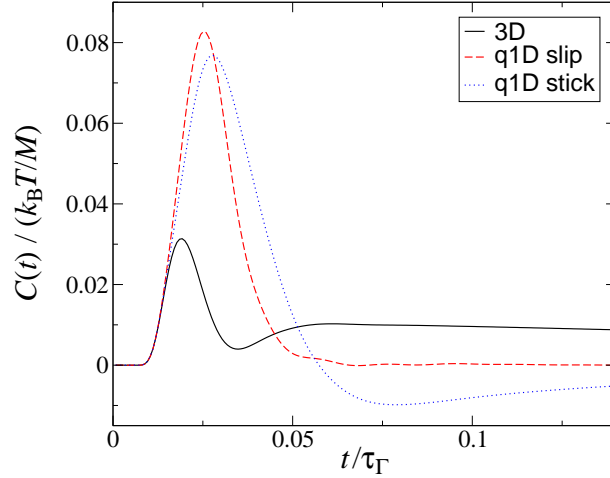


Figure 4. Velocity cross-correlation functions for two particles, as obtained from lattice-Boltzmann simulations of three systems: an unbounded fluid, a fluid in a square channel (side h) with slip boundary conditions, and a fluid in a square channel with no-slip boundary conditions. The particles have diameter σ and mass M and they are separated by a distance $d = 2\sigma = 1.33h$. The time unit is $\tau_\Gamma = h^2/\Gamma$.

particle. This signal is suppressed with increased separation because of sound diffusion. It is followed by a long-time negative algebraic tail, whose magnitude does not show any dependence on separation. On the one hand, this indicates a correlation of *unrestricted spatial range*. On the other hand, the backflow associated with the negative tail causes the particle to return almost exactly to its initial position; the time-integrated correlation (which is equal to the coupling diffusion coefficient of the particle pair) decays exponentially with d/h . This is how the two phenomena—long-range temporal correlations and short-range steady-state correlations—are reconciled.

To quantitatively account for the long-time algebraic behavior of the correlations we need to relate the diffusive density perturbation, given by Eq. (14), to the flow velocity. This can be done either via the continuity equation, $\partial_t \delta\rho = -\rho_0 \partial_x u$, or by applying Fick’s law to the sound diffusion, $\rho_0 u = -D_s \partial_x \delta\rho$. Both methods yield the same long-time flow velocity,

$$u(x, t) = -\frac{b}{4c_s h \rho_0 \sqrt{\pi \alpha \nu}} \left(\frac{1}{t} \right)^{3/2}.$$

Equating it with the velocity advecting particle 2 and applying the fluctuation-dissipation theorem, as explained above, we obtain the long-time velocity cross-correlation function [23],

$$C(t, d) = -\frac{k_B T}{4c_s h \rho_0 \sqrt{\pi \alpha \nu}} \left(\frac{1}{t} \right)^{3/2}, \quad (15)$$

which has no dependence on the inter-particle separation d . The negative sign of the long-time tail is traced back to the dipolar shape of the diffusive density perturbation, Eq. (14).

4. Collective dynamics

Finally, we study the effect of sound on the collective dynamics of many particles. The discussion in this section is restricted to the q1D geometry of a rigid channel with no-slip boundary conditions.

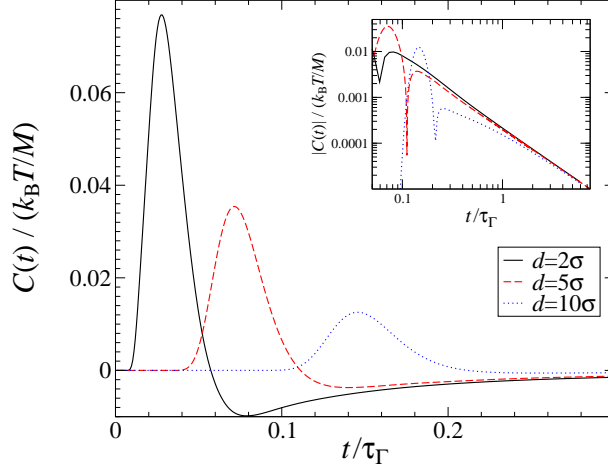


Figure 5. Velocity cross-correlation functions for two particles in a rigid channel (no-slip boundary conditions), as obtained from lattice-Boltzmann simulations. The particles, situated on the channel axis, have diameter σ and mass M . The channel has a square cross-section of side $h = 1.5\sigma$. Correlations are shown for three different inter-particle separations. The time unit is $\tau_\Gamma = \hbar^2/\Gamma$. The inset shows the absolute value of the correlations on a logarithmic scale, demonstrating the $(-3/2)$ power law at long times, with a distance-independent amplitude.

We consider the wavenumber-dependent particle current correlation function [22],

$$J(k, t) = \frac{1}{N} \sum_{i,j} \left\langle V_i(0) V_j(t) e^{ik(x_i(0) - x_j(t))} \right\rangle, \quad (16)$$

where N is the number of particles and i, j are particle labels. Self-contributions to the sum, with $i = j$, are related to the velocity autocorrelation function of single particles, $\langle V(0)V(t) \rangle$. As our interest here lies solely in cross-correlations, we subtract this contribution and consider $J_c(k, t) = J(k, t) - \langle V(0)V(t) \rangle$.

To obtain J_c from lattice-Boltzmann simulations we assume time-scale separation between the relaxation of the fluid and that of particle configurations. We generate configurations X^N of N particles using a Monte Carlo scheme. For each configuration we assign to each particle an initial velocity from a Maxwell-Boltzmann distribution and then follow the time evolution of every particle in a lattice-Boltzmann simulation. This allows us to calculate, for each configuration, the velocity cross-correlation functions between all pairs of particles, $\langle V_i(0)V_j(t) \rangle_{\{X^N\}}$, as described in Sec. 3. The assumption of time-scale separation simplifies the expression for J_c to

$$J_c(k, t) = \frac{\phi}{\sigma} \int_{-\infty}^{\infty} dx g(x) e^{ikx} \left\langle V_1(0) V_2(t) \right\rangle_{\text{fast}} \{x\},$$

where $g(x)$ is the equilibrium pair correlation function of the particles, and $\phi = N\sigma/L$ (L being the channel length) is their linear fraction. The angular brackets $\langle \dots \rangle_{\text{fast}}$ denote a double averaging procedure: first, for a given configuration, an average is taken over time that is sufficiently long for the fluid to relax but sufficiently short for the configuration to be considered “frozen”; then another averaging is performed over many particle configurations with the constraint $x_1 - x_2 = x$.

In Fig. 6 we plot the time evolution of $J_c(k, t)$, thus obtained from the lattice-Boltzmann simulations, for various wavenumbers k . As $t \rightarrow 0$, J_c vanishes, as the inter-particle correlations

in the compressible fluid require a finite time to develop. The presence of oscillations for small wavelengths, comparable to the particle size and channel width, reflects the wave-like propagation of sound over these small length scales. The oscillations vanish at longer wavelengths, indicating the onset of diffusive sound propagation. At long times, the particle current correlation J_c decays algebraically as $t^{-3/2}$.

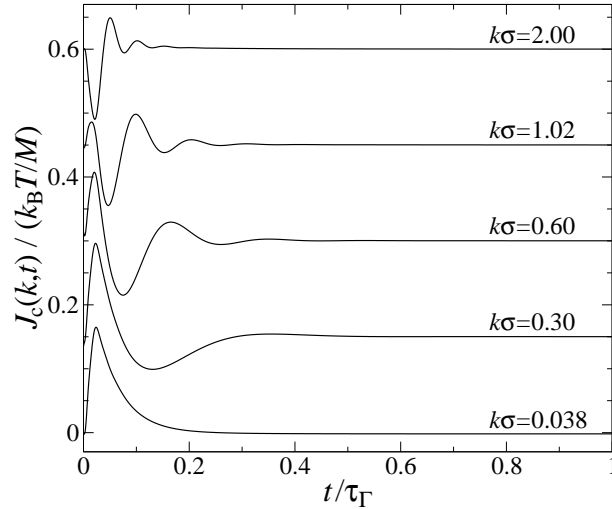


Figure 6. Particle current correlation functions obtained from lattice-Boltzmann simulations for a suspension of particles (diameter σ , linear fraction $\phi = 0.72$) in a square channel (side $h = 1.5\sigma$). The different curves, corresponding to different wavenumber k , are shifted vertically by 0.15 from each other, for clarity. The time unit is $\tau_\Gamma = h^2/\Gamma$.

To further clarify the results of Fig. 6 we resort to a simple model, where $g(x)$ is replaced by its dilute limit: $g(x) = 0$ for $|x| < \sigma$, and $g(x) = 1$ for $|x| > \sigma$. For the velocity cross-correlation function $\langle V_1(0)V_2(t) \rangle_{\text{fast}}\{x\}$ we use the 1D description of Sec. 3. From Eq. (11) and the continuity equation, $\partial_t \delta \rho_k = -ik \rho_0 u_k$, we obtain the flow velocity u_k . The fluctuation-dissipation theorem is then used to relate the flow to the velocity cross-correlations. This model yields

$$\frac{J_c(k, t)}{k_B T} = \frac{\phi}{b\sigma} \left[u_k(t) - \int_{-\sigma}^{\sigma} dx e^{-ikx} u(x, t) \right]. \quad (17)$$

The qualitative change in J_c as its oscillations vanish at long wavelengths is reproduced by the first term. The onset of the overdamped diffusive regime for small wavenumbers, lying outside the range delineated in Eq. (12), should occur for the parameters used in the simulation at $k\sigma < 0.18$, which is in line with Fig. 6. The second term in Eq. (17) supplies the function J_c with the algebraic decay $\sim t^{-3/2}$, which at long wavelength is positive.

Another function that characterizes the collective dynamics of particles is the dynamic structure factor [22, 24],

$$S(k, t) = \frac{1}{N} \sum_{i,j}^N \left\langle e^{ik(x_i(0) - x_j(t))} \right\rangle. \quad (18)$$

At times much shorter than the configurational relaxation time it decays exponentially with time and can be written as

$$S(k, t) = S_0(k) e^{-tk^2 H(k)/S_0(k)},$$

where $S_0(k) = S(k, t = 0)$ is the static structure factor. The hydrodynamic factor $H(k)$ accounts for the effect of fluid-mediated correlations on the dynamic structure and is given by [24]

$$H(k) = D_{\text{self}} + \frac{1}{N} \sum_{i \neq j}^N \left\langle D_{ij} \{X^N\} e^{ik(x_i - x_j)} \right\rangle,$$

where $D_{ij} \{X^N\}$ are the configuration-dependent pair diffusion coefficients, and $D_{\text{self}} = \langle D_{ii} \rangle$ is the self-diffusion coefficient. Note that $H(k)$ depends only on steady-state properties of the fluid and, hence, is unaffected by sound.

Recalling the Green–Kubo relation [22],

$$D_{ij}(x) = \int_0^\infty dt \left\langle V_i(0) V_j(t) \right\rangle \{x\},$$

and assuming time-scale separation, we relate $H(k)$ to the current correlation function,

$$H(k) = \int_0^\infty dt J(k, t).$$

To examine the effect of sound we therefore use the functions

$$\hat{H}(k, t) = \int_0^t dt' J(k, t'), \quad \hat{H}_c(k, t) = \int_0^t dt' J_c(k, t'),$$

such that in the limit $t \rightarrow \infty$ $\hat{H}(k, t)$ reduces to $H(k)$, and $\hat{H}_c(k, t)$ to $H(k) - D_{\text{self}}$ [25]. Figure 7 shows the dependence of $\hat{H}(k, t)$ on k at various times. As t increases, $\hat{H}(k, t)$ converges to its limiting form, $H(k)$, and eventually all sound effects vanish. However, at any finite time there appears a feature that is absent in unbounded suspensions—a sharp peak at $k \rightarrow 0$.

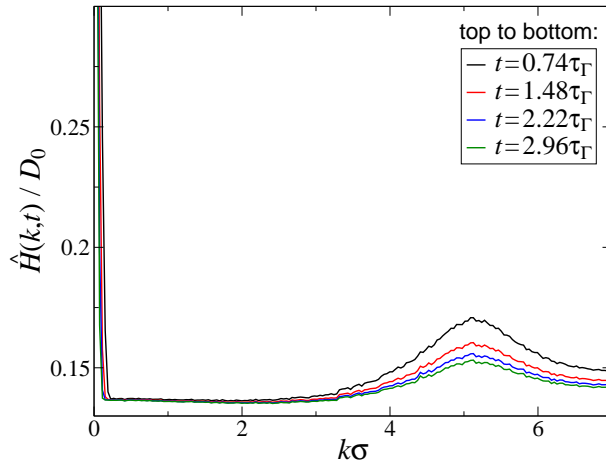


Figure 7. Temporal hydrodynamic factor as a function of wavenumber at various times. The system is the same as in Fig. 6.

To see that the small k feature is due to long-range sound-mediated correlations, we return to the simplified 1D description. Using Eq. (17) and the continuity equation, $\partial_t \delta \rho_k = -ik \rho_0 u_k$, we obtain

$$\frac{\hat{H}_c(k, t)}{k_B T} = \frac{\phi}{b \sigma \rho_0} \left[\frac{\delta \rho_k(t)}{(-ik)} - \frac{1}{\pi} \int_{-\infty}^{\infty} dk' \frac{\sin(\sigma(k' - k))}{k' - k} \frac{\delta \rho_{k'}(t)}{(-ik')} \right], \quad (19)$$

where $\delta\rho_k$ is given by Eq. (11) [or by Eq. (13) for small k]. At $t \rightarrow \infty$ this expression vanishes, indicating that within the simplified 1D description all steady correlations between particles confined in the channel disappear, and $H(k) = D_{\text{self}}$. However, at any finite t , we have a range of small wavenumbers, $k^2 < (D_s t)^{-1}$, for which Eq. (19) reduces to

$$\frac{\hat{H}_c(k, t)}{D_0} \approx \frac{3\pi\phi}{\alpha} \left(e^{-D_s k^2 t} - \frac{\sigma}{\sqrt{\pi D_s t}} \right), \quad (20)$$

where $D_0 = k_B T / (3\pi\eta\sigma)$ is the Stokes-Einstein self-diffusion coefficient in an unbounded fluid. Equation (20) contains two interesting terms originating from sound diffusion. The first contributes at $k \rightarrow 0$ a *time-independent* constant. The second adds a *k-independent* negative long-time algebraic tail, $\sim (-t^{-1/2})$, which derives from the time-integrated $t^{-3/2}$ tail of the current correlation function $J_c(k, t)$.

In Fig. 8 we replot the function $\hat{H}(k, t)$, focusing on the small k region, and compare it with the fit $\frac{\hat{H}(k, t)}{D_0} = \frac{6\pi\phi}{\alpha} e^{-D_s k^2 t}$ [21]. The agreement between theory and simulation is satisfactory, both exhibiting the small- k peak.

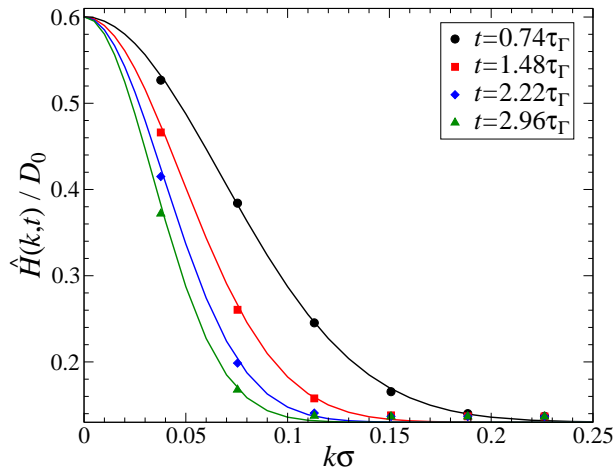


Figure 8. Temporal hydrodynamic factor for small wavenumber at various times. The system is the same as in Fig. 6. Data points represent lattice-Boltzmann simulation results. Solid lines show the expression $\frac{\hat{H}(k, t)}{D_0} = \frac{6\pi\phi}{\alpha} e^{-D_s k^2 t}$.

5. Conclusion

In the present work we have tried to establish the role of fluid density perturbations (sound) in mediating dynamic correlations among particles in a channel at the pair and the collective levels. We have been motivated in this investigation by two considerations: (i) the hydrodynamic effects that are not associated with sound (due to momentum and steady pressure) are screened in a rigid channel and have no bearing on long-range particle correlations; (ii) the density perturbations in a channel do not decay within a well defined relaxation time (as in an unbounded fluid) but rather relax algebraically, thus giving sound a long memory.

The effects of sound on particle correlations in a rigid channel have been found to be quite striking. At the two-particle level, the velocity cross-correlation function is independent of inter-particle distance (i.e., unrestricted in its range) and has a long-time negative algebraic tail $\sim (-t^{-3/2})$ (similar to the single-particle autocorrelation function [5, 6, 7]). At the collective level of a large particle assembly (q1D suspension), the particle current correlation function has

a similar long-time algebraic tail. We have characterized the collective correlations by a time-dependent hydrodynamic factor, $\hat{H}_c(k, t)$, which converges to the ordinary hydrodynamic factor at infinite time [25]. The sound-mediated correlations in the channel make this function exhibit an anomalous peak at small wavenumbers and a long-time algebraic temporal decay $\sim (-t^{-1/2})$. Thus, in summary, the common picture of negligible, exponentially screened hydrodynamic interactions among particles in a rigid channel is somewhat misleading; strictly speaking, it applies only at steady state.

At the same time, the predicted sound-mediated correlations are weak and may be measurable only over sufficiently short times. The correlation is inversely proportional to the speed of sound [see, e.g., Eq. (15)], which makes its amplitude small, and the sound diffusion is fast — for water in a micron-wide channel, $D_s = c_s^2 h^2 / (\alpha \nu) \sim 0.1 \text{ m}^2/\text{s}$. For example, let us examine the correlation between the observable Brownian displacements of two distant particles along the channel, as characterized by their pair diffusivity,

$$D_{12}(t) \equiv \frac{\langle \Delta x_1 \Delta x_2 \rangle}{2t} = \frac{1}{t} \int_0^t dt' \int_0^{t'} dt'' C(t'', d) = \frac{k_B T}{c_s h \rho_0 \sqrt{\pi \alpha \nu}} t^{-1/2}. \quad (21)$$

For a micron-wide channel filled with water, according to Eq. (21), measuring D_{12} of order $10^{-3} \text{ } \mu\text{m}^2/\text{s}$ would require a temporal resolution of order 10^{-7} s . Thus, the predicted sound-mediated effects might be observable using experimental techniques of high temporal and spatial resolution, such as diffusive wave spectroscopy [12] or fast optical tracking [14, 26]. The fact that D_{12} is independent of inter-particle distance may greatly facilitate the acquisition of statistics in such fast-tracking experiments.

The short-time relevance of sound-mediated correlations was noted in earlier works on unconfined suspensions [12, 13, 14]. We end by underlining the key differences between those correlations and the ones in a rigid channel addressed here. First, whereas in an unconfined suspension sound propagates as an underdamped wave until it is scattered by a sufficient number of particles [12], in a channel, because of scattering from the boundaries, sound becomes diffusive as soon as the distance gets much larger than the channel width. Second, in an unconfined suspension sound-mediated correlations are a sub-dominant effect, quickly taken over by vorticity diffusion (transverse modes) [12, 13]. By contrast, in a rigid channel correlations due to transverse flow are cut off, leaving longitudinal flow as the sole mechanism of long-range correlations. Thus, any correlation which could be resolved at inter-particle distances much larger than the channel width should be associated with sound-mediated effects.

Acknowledgments

This research has been supported by the Israel Science Foundation (Grants No. 588/06 and No. 8/10).

References and Notes

- [1] Happel J and Brenner H 1983 *Low Reynolds Number Hydrodynamics* (The Hague: Martinus Nijhoff)
- [2] Cui B, Diamant H and Lin B 2002 *Phys. Rev. Lett.* **89** 188302
- [3] Brinkman H C 1949 *Appl. Sci. Res. A* **1** 27
- [4] Ramaswamy S and Mazenko G F 1982 *Phys. Rev. A* **26** 1735
- [5] Hagen M H J, Pagonabarraga I, Lowe C P and Frenkel D 1997 *Phys. Rev. Lett.* **78** 3785
- [6] Pagonabarraga I, Hagen M H J, Lowe C P and Frenkel D 1998 *Phys. Rev. E* **58** 7228
- [7] Pagonabarraga I, Hagen M H J, Lowe C P and Frenkel D 1999 *Phys. Rev. E* **59** 4458
- [8] Frydel D and Rice S A 2007 *Phys. Rev. E* **76** 061404
- [9] Felderhof B U 2011 *J. Chem. Phys.* **134** 024505
- [10] Cui B, Diamant H, Lin B and Rice S A 2004 *Phys. Rev. Lett.* **92** 258301
- [11] Diamant H 2009 *J. Phys. Soc. Jpn.* **78** 041002
- [12] Ladd A J C, Gang H, Zhu J X and Weitz D A 1995 *Phys. Rev. E* **52** 6550

- [13] Bakker A F and Lowe C P 2002 *J. Chem. Phys.* **116** 5867
- [14] Henderson S, Mitchell S and Bartlett P 2002 *Phys. Rev. Lett.* **88** 088302
- [15] Felderhof B U 2010 *J. Fluid Mech.* **644** 97
- [16] Frydel D and Diamant H 2010 *Phys. Rev. Lett.* **104** 248302
- [17] Navardi S and Bhattacharya S 2010 *J. Math. Phys.* **51** 043102
- [18] Felderhof B U 2010 *Physica A* **389** 5602
- [19] Felderhof B U 2011 *J. Fluid Mech.* **668** 100
- [20] Landau L D and Lifshitz E M 1987 *Fluid Mechanics* 2nd edition (Pergamon: Oxford)
- [21] The fields (density, flow velocity) in the 1D model correspond to cross-sectional averages of the actual fields, whereas in the simulation we measure quantities at the center of the channel. This makes the simulation result larger than the analytical one by a factor of ≈ 2 . (For a parabolic velocity profile in a circular tube the cross-sectional average is exactly 1/2 the central value [9].)
- [22] Hansen J P and McDonald I R 1986 *Theory of Simple Liquids* 2nd edition (London: Elsevier)
- [23] Because of cross-sectional averaging [21], this result of the 1D model is smaller than the corresponding long-time behavior in the simulations by a factor of ≈ 4 . The additional factor of ≈ 2 arises from the continuity equation (or Fick's law), relating the cross-sectional averages of density (a roughly uniform transverse profile) and velocity (a roughly parabolic profile).
- [24] Pusey P N 1991 in *Liquids, Freezing and Glass Transition II* eds J P Hansen, D Levesque and J Zinn-Justin (Amsterdam: Elsevier) pp 763–942
- [25] A time-dependent hydrodynamic factor was introduced before, using a different definition [12]. The relation between our function, $\hat{H}_c^{(2)}$, and the one used in Ref. [12], $\hat{H}_c^{(1)}$, is $\hat{H}_c^{(1)}(k, t) = t^{-1} \int_0^t dt' \hat{H}_c^{(2)}(k, t')$.
- [26] Huang R, Chavez I, Taute K M, Lukić B, Jeney S, Raizen M G and Florin E-L 2011 *Nat. Phys.* **7** 576